Mixed Proton and Electron Conducting Double Perovskite Anodes for Stable and Efficient Tubular Proton Ceramic Electrolysers

Einar Vøllestad[1,3], Ragnar Strandbakke[1], Mateusz Tarach[2], David Catalán[2], Marie-Laure Fontaine[3], Dustin Beeaff[4], Daniel R. Clark[1,4], Jose M. Serra[2], Truls Norby[1,*]

[1]Department of Chemistry, University of Oslo, FERMiO, Gaustadalléen 21, NO-0349 Oslo, Norway

[2]Instituto de Tecnología Química (Universitat Politècnica de València - Consejo Superior de Investigaciones Científicas), Avenida de los Naranjos s/n.46022 Valencia, Spain

[3]SINTEF Industry, NO-0314 Oslo, Norway

[4]CoorsTek Membrane Sciences AS, Gaustadalléen 21, NO-0349 Oslo, Norway

Hydrogen production from water electrolysis is a key enabling energy storage technology for large scale deployment of intermittent renewable energy sources. Proton Ceramic Electrolysers (PCEs) can produce dry pressurized hydrogen directly from steam, avoiding major parts of cost-driving downstream separation and compression. The development of PCEs has however suffered from limited electrical efficiency due to electronic leakage and poor electrode kinetics. Here, we present the first fully-operational $BaZrO_3$-based tubular PCE, with 10 cm^2 active area and a hydrogen production rate above 15 $NmL \cdot min^{-1}$. The novel steam anode $Ba_{1-x}Gd_{0.8}La_{0.2+x}Co_2O_{6-\delta}$ (BGLC) exhibits mixed p-type electronic and protonic conduction and low activation energy for water splitting, enabling total polarization resistances below 1 $\Omega \cdot cm^2$ at 600°C and faradaic efficiencies close to 100% at high steam pressures. These tubular PCEs are mechanically robust, tolerate high pressures, allow improved process integration, and offer scale-up modularity.

High temperature electrolysers (HTEs) that utilize readily available steam and/or heat (renewable or industrial) as a supplementary energy source provide superior electrical efficiency compared to conventional water electrolysis.[1-4] HTEs developed to date comprise solid oxide electrolysers (SOEs) which utilize oxide ion conducting electrolytes and therefore produce hydrogen on the steam side cathode. The undiluted high pressure oxygen produced on the anode in SOEs presents a safety hazard. Their high operating temperature (typically 800°C)

imposes challenges in terms of cell degradation, expensive construction materials, and constrained process integration.[4-6] Operation at temperatures below 700°C would reduce degradation and enable the utilization of inexpensive stainless steel materials in manifolds and housing for pressurized systems.[7]

Proton ceramic electrolysers (PCEs) based on proton conducting electrolytes such as Y-doped $BaZrO_3$-$BaCeO_3$ solid solutions (BZCY) conversely transport protons (H^+) from the steam anode to the hydrogen-side cathode. Unlike other electrolysers it hence produces directly dry electrochemically pressurized H_2 at the cathode while the O_2 produced at the anode is diluted with steam (

Figure *1*a).[8-11] This reduces the risks of handling undiluted oxygen at high pressure and temperature and more importantly alleviates the necessity for most of the cost-driving downstream separation and mechanical compression of H_2, amounting for instance to approximately 2.4 and 3 kWh/kg H_2 at 600°C for compression ratios of 10 and 20, respectively. PCEs instead offer the direct production of pressurized H_2 from low-pressure steam, and the associated compression heat can be locally utilized in the endothermic electrolysis reaction at the cathode, in turn giving rise to higher process energy efficiency. Protons migrate with lower migration barrier than oxide ions, and are thus favourable for operation at intermediate temperatures, e.g. 400-700°C, which is suitable for integration with renewable heat sources (solar-thermal and geothermal plants), and waste heat from industrial plants.

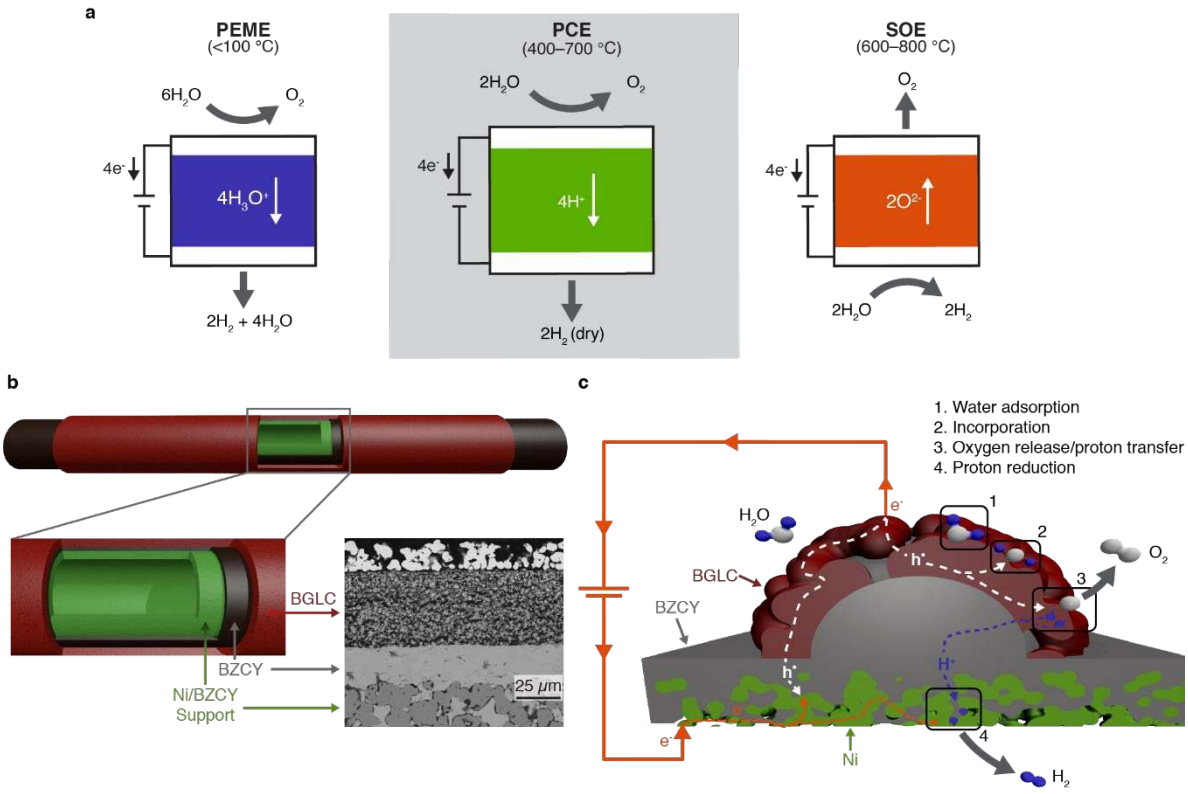

Figure 1: | Schematics of water electrolysis technologies and PCE membrane and transport. a, Comparison of PEME, PCE and SOE operation, illustrating the benefit of PCEs with production of undiluted dry hydrogen on the cathode and diluted oxygen on the anode. **b,** Illustrations of a tubular PCE architecture producing dry hydrogen in the inner cathode chamber with scanning electron micrograph of a polished cell architecture. **c,** Detailed view of transport phenomena and reaction mechanisms through a PCE.

The promise of proton ceramic technologies have recently been demonstrated for highly performing and fuel-flexible fuel cells (PCFCs),[12-14] tubular proton ceramics for direct methane conversion into benzene[15] and intensified steam methane reforming.[16] However, reports of steam electrolysis are scarce and limited to laboratory-scale button cells (< 0.5 cm^2) with moderate performance and low efficiencies (40-60%).[17-21] So far, a lack of efficient and stable steam anodes have caused high overpotentials that impose increased p-type electronic conductivity in the BZCY electrolyte, resulting in electronic leakage currents and reduced faradaic efficiency, typically below 50%. Herein, we show how these materials-specific challenges can be addressed and overcome to reach satisfactory efficiencies close to 100%, and how targeted adjustment of the anode material composition enables outstanding and stable operation of tubular PECs (**Figure *1***) at high steam pressures.

The anode activity towards the electrochemical oxygen-steam redox reaction can be enhanced by extending the reaction zone beyond the triple phase boundaries (tpb) through the use of mixed *protonic electronic* conductors (MPECs) as electrode material (**Figure *1***c). For a long time, materials that combine mixed *protonic* and electronic conduction with high catalytic activity and thermodynamic stability have been notoriously elusive. However, recent efforts have led to the discovery of electronically conductive perovskite-based materials that exhibit proton incorporation in the presence of steam.[13,22-25] Among these, the double perovskite $BaGd_{0.8}La_{0.2}Co_2O_{6-\delta}$ (BGLC) exhibits the lowest apparent polarisation resistance reported for proton ceramic cells of 0.05 $\Omega \cdot cm^2$ at 650°C in a symmetrical cell with wet air ($E_A < 50$ kJ·mol^{-1}) for the oxygen-steam redox reaction, and an electronic conductivity higher than 800 Scm^{-1}.[23,26,27] BGLC is an ordered double perovskite with oxygen vacancies preferentially located in the lanthanide-layer, and displays considerable proton incorporation in humid atmospheres.[23] A recent molecular dynamics study[28] of a similar compound, $BaGdCo_2O_{5+\delta}$, revealed fast proton diffusion kinetics within the a-b plane, supporting the mixed protonic conduction character of BGLC electrodes. For the purpose of high pressure electrolysis, where the anode material is exposed to high pH_2O, we tailored the composition of BGLC by partial substitution of Ba with La, giving the general formula $Ba_{1-x}Gd_{0.8}La_{0.2+x}Co_2O_{6-\delta}$. Stability tests at 600°C under 1.5 bar of steam for 72 hours showed a separation into two phases for compositions with $x < 0.5$, i.e., a double perovskite phase and hexagonal $BaCoO_3$ (Supplementary Information (SI) Fig.1).[29] Precipitation of $BaCoO_3$ proceeds until the remaining double perovskite phase reaches a composition stable in steam, thereafter the two phases coexist under the given conditions (**Figure *2***). The stable double perovskite phase is expected to have both of the two lanthanides substituted for Ba. Indeed, XRD analysis shows that when 50% of the Ba is substituted with La (x = 0.5), BGLC is stable in 1.5 bar of steam, with no precipitation of $BaCoO_3$. The excellent stability in high steam atmospheres was further confirmed at a pressure of 28 barg (75% steam 25% O_2) at 600°C with no evidence of secondary phase formation (SI Fig. 1c).

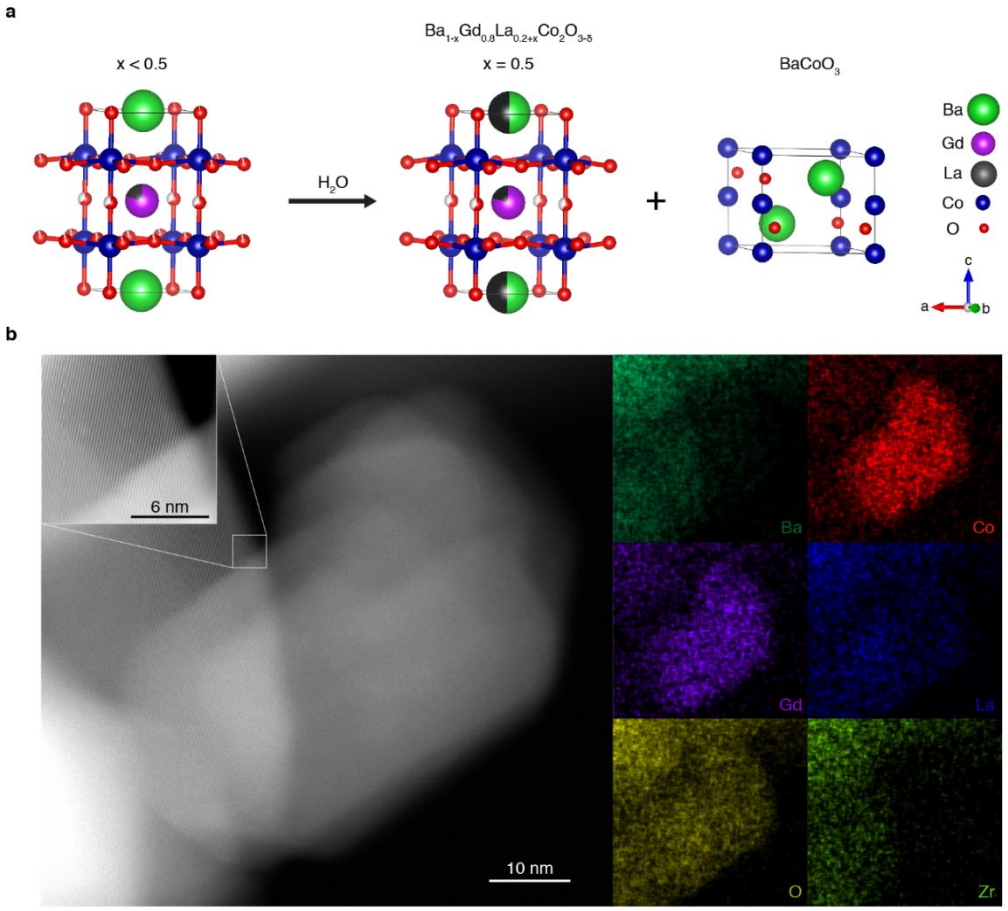

Figure 2: Phase segregation and microscopy of BGLC. a, Phase segregation and stability of BGLC in 1.5 bar of steam and 600°C after 72 hours. **b,** S/TEM analysis of BGLC nanoparticle after operation as steam anode. High-angle annular dark-field (HAADF) micrograph on the left with corresponding energy dispersive x-ray spectroscopy (EDS) maps of Ba, Co, Gd, La, O and Zr. High-resolution S/TEM micrograph of interface in the top left.

Tubular PCEs were assembled by brush-painting 30 µm-thick BGLC-based anodes on 6 cm long tubular BZCY-NiO/BZCY half-cells. The half-cells were produced by co-sintering spray-coated BZCY electrolyte on extruded Ni/BZCY cathode support tube using solid-state reactive sintering.[30] This method ensures a reproducible, cost-efficient and highly scalable[15,16] production route of open-ended tubular segments with 5-10 cm^2 active area. BZCY72 ($BaZr_{0.7}Ce_{0.2}Y_{0.1}O_{2.95}$) was chosen as the electrolyte composition as a compromise between thermodynamic stability (high Zr content) and low grain boundary resistance (high Ce content). Composite BGLC/BZCY anodes were also employed to tailor the macroscopic thermal expansion of the electrode layer to better match that of the tubular support, which is critical to achieve sufficient attachment and mechanical integrity in tubular systems during thermal cycling. **Figure *1***b-c shows a schematized cell arrangement and a detailed SEM view of the electrodes-electrolyte interfaces and the top Pt current collector. Details on cell manufacturing

are given in Supplementary Information (SI). BGLC and BZCY phases are chemically compatible as confirmed by XRD analysis of co-fired powders and form clean grain interfaces, as revealed by S/TEM analysis of composite anodes after electrolysis tests at high steam pressures (**Figure *2***b).

Figure *3*a displays current-voltage behaviour of cells operated under electrolytic bias at a total pressure of 3 bar, with 1.5 bar steam and 80 mbar O_2 on the anode side and 0.3 bar H_2 on the cathode side (Ar as balance on both sides) at 600°C. The cells with the composite anode displayed the lowest total area-specific resistance (ASR) under operation, and much higher faradaic efficiencies. Electrochemical impedance analysis under slight electrolytic bias (**Figure *3***b) reveals a significantly lower electrode polarization resistance (R_p) for the composite anode (0.8 $\Omega \cdot cm^2$) as compared to the single-phase BGLC anode (4 $\Omega \cdot cm^2$). Post-measurement inspections of the single-phase BGLC anode revealed considerable delamination of the electrode layer, and the larger impedance of this cell is thus attributed to poor adhesion and limited reaction zone between the electrode and electrolyte resulting from TEC-mismatch between BGLC and the Ni/BZCY support. This was successfully mitigated by using composite anodes, where a combination of higher annealing temperature and improved TEC-matching with the tubular support ensured a mechanically robust electrode layer with good adhesion to the electrolyte.

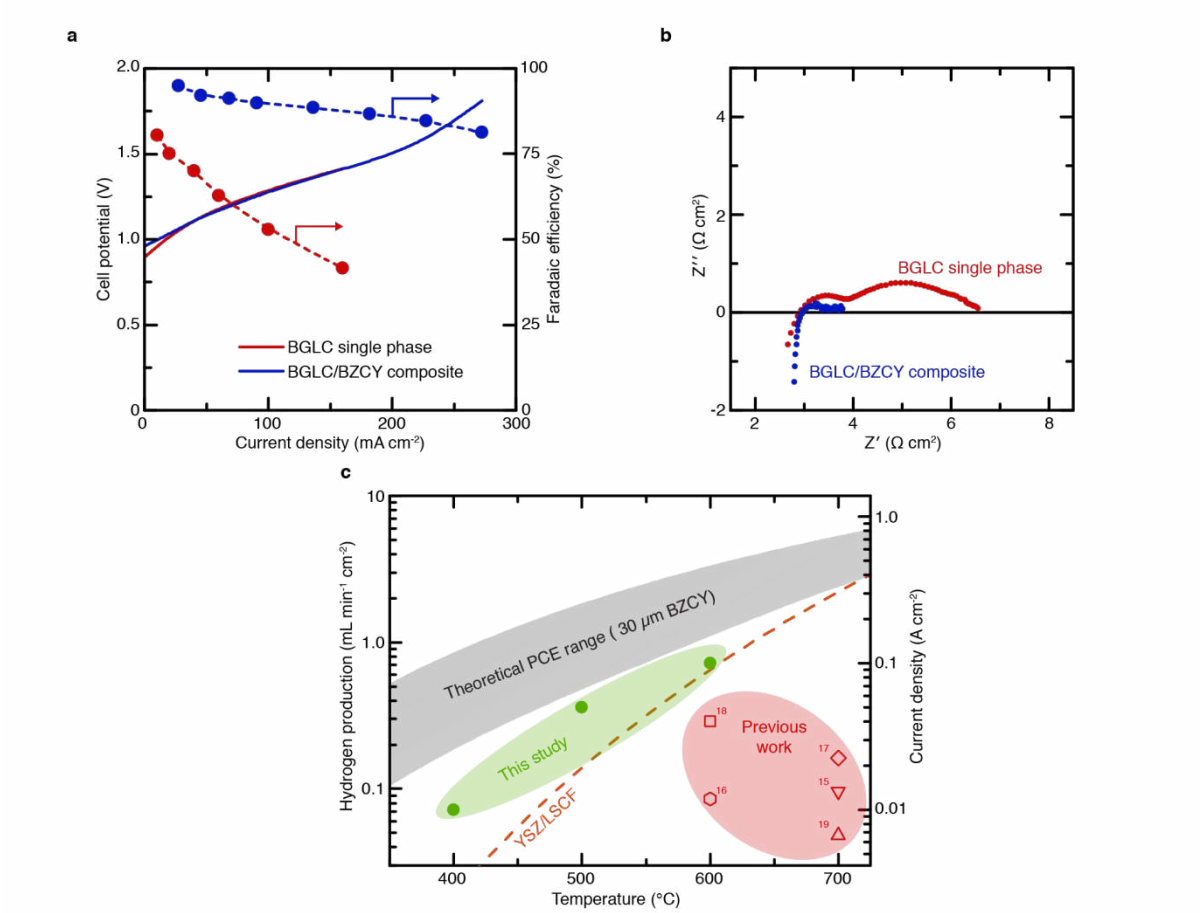

Figure 3: PCE electrochemical performance and literature comparison. a, Current-voltage curves and faradaic efficiency of two different PCEs measured at 600°C with 1.5 bar steam in the anode compartment. **b,** Corresponding Nyquist plots of the two cells under a small electrolytic bias. **c,** Hydrogen production rates and ionic current densities at thermo-neutral voltage (1.29 V) compared to literature values calculated from reported area specific resistances and faradaic efficiencies. The grey area provides the theoretical range of operation for PCEs considering a 30 µm thick BZCY electrolyte with BGLC anode. The dashed line represents predicted SOE performance using 30 µm thick YSZ electrolyte with LSCF anode.

The polarisation resistance of the composite anode cell under electrolytic operation is below 1 $\Omega \cdot cm^2$ for anode and cathode combined at 600°C with an activation energy of 0.4 eV between 400 and 700°C (SI, Fig. 11) attributed primarily to the BGLC steam anode. The rate limiting step for the water splitting anode reaction is ascribed to surface-related processes (adsorption, dissociation and diffusion) as inferred from the capacitance values of 10^{-4}-10^{-2} $F \cdot cm^{-2}$, in agreement with our previous work on BGLC.[23] In addition, gas phase diffusion resistance (with associated capacitances of 1-10 $F \cdot cm^{-2}$) accounts for around 1/3 of R_p at 600°C. Upon increasing electrolytic bias, however, gas diffusion resistance diminishes, indicating that consumption and thereby reduction of H_2O levels facilitate desorption and diffusion of the formed molecular oxygen, i.e., that high steam pressures correspondingly cause oxygen mass transfer limitations

at low currents. The ohmic resistance is a major contributor to the total cell resistance, and includes also parasitic contact and current collection resistances resulting from the large electrode area of the measurement setup and tubular geometry. ASR values are given without scaling parasitic wiring and contact resistances to the total area (see SI for details). The robustness of the composite electrode processing was further investigated across four cells employing different current collection and manufacturing process, showing only small variations in electrode polarization (cf. SI Fig. 6). There was, however, significant differences in the ohmic offset of the cells due to parasitic and contact resistances arising from the different current collection approaches, highlighting the challenge of current collection along the length of tubular electrochemical cells.

By implementing stable BGLC and BZCY compositions as the anode and electrolyte materials, we have been able to produce fully operational PCEs with larger surface areas (>10 cm^2) that can be operated close to 100% faradaic efficiency at 500-600°C under high steam pressures. The H_2-production rates of these tubular cells under thermo-neutral operation (1.29 V) exceed those in the literature using small button-cell PCEs, as shown in **Figure *3***c.[17-21] H_2 production rates obtained in this work approach the predicted range of PCE operation considering a 30 µm thick BZCY and BGLC as the anode[23,26] and surpass that of SOE operation below 700°C with YSZ and LSCF as the electrolyte and anode, respectively (See SI for details).[31-33] Reducing the electrolyte thickness below our present 30 µm is well possible and would lower the ASR and increase H_2 production rates considerably further.

The reported hydrogen production rates of button-cell electrolysers in the literature deviate significantly from the theoretical performance of PCEs,[17-21] principally due to low faradaic efficiencies (η_F < 50%) originating from severe p-type electronic leakage through the electrolyte induced by large anode overpotentials. To illustrate the issue of leakage currents, the transport of the protonic and electronic (holes and electrons) charge carriers can be understood to proceed in "rails" connected in parallel (**Figure *1***c and SI Fig. 13) where each carrier displays a particular dependency on cell potential, temperature and partial pressures. In these rails, protons must overcome three in-series connected resistances – ascribed to anode, electrolyte and cathode – while electronic charge carriers depend on the electronic conductivity in the electrolyte only.

Imposing higher current densities in electrolysis operation leads to higher cell potentials that in turn induces the generation of additional p-type electronic charge carriers in the electrolyte on

the anode interface.[34 35] In proton conducting BZCY ceramics, the concentration of electron holes can be related to oxygen and steam partial pressures and the redox potential *E* through the water oxidation equilibrium as

$$[\mathrm{h}^{\bullet}] = K_{\mathrm{ox}}[\mathrm{OH}_{\mathrm{O}}^{\bullet}]p_{\mathrm{H_2O}}^{-\frac{1}{2}}\, p_{\mathrm{O_2}}^{\frac{1}{4}} = K_{\mathrm{ox}}\exp\left(\frac{F(E-E^0)}{RT}\right) \quad (1)$$

, assuming full hydration of BZCY ($[\mathrm{OH}_{\mathrm{O}}^{\bullet}] = [\mathrm{Y}_{\mathrm{Zr}}^{/}]$). Thus, operation of a PCE anode at high potentials effectively enhances the electronic leakage current (and lowers faradaic efficiency η_F). Similarly, increased n-type conduction develops on the cathode-electrolyte interface as the cathode overpotential increases and the effective hydrogen pressure is increased.

High-steam pressure operation will shift the equilibrium towards lower electron hole concentration, higher proton concentration, and thus a higher ionic transport number near the anode. At a fixed steam utilization rate, increased total pressure should diminish the hole concentration with a $p_{\mathrm{tot}}^{-1/4}$-dependency, giving rise to higher efficiency η_F. Lower temperature increases the efficiency further due to decreased hole and increased proton concentrations, helped by the low activation energy for water oxidation by the BGLC anode, as illustrated in **Figure *4***a, where I-V-characteristics and H_2 production rates at 500, 600, and 700°C are presented for the composite anode cell.

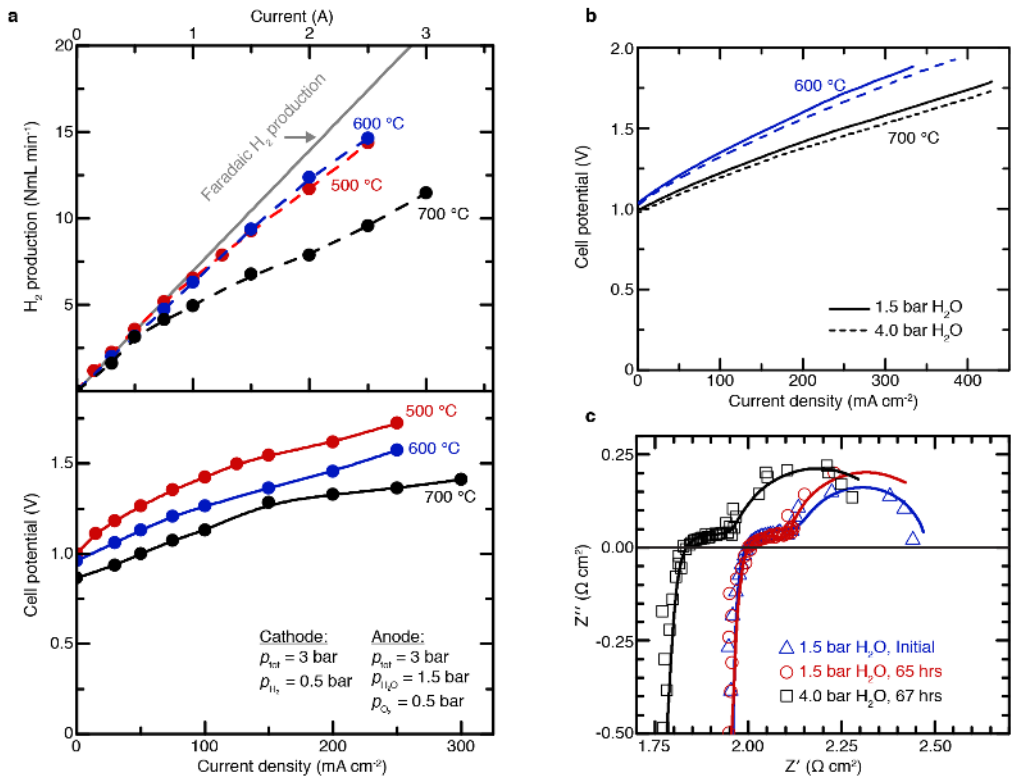

Figure 4: PCE cell performance and characterization. a, Hydrogen production and current-voltage relations of a composite-anode cell at 500, 600 and 700°C operated at 1.5 bar steam. **b,** Current-voltage relations at 600 and 700 °C in 1.5 and 4 bar steam using a 10 cm^2 composite anode. **c,** Impedance sweeps at 700°C and 1.5 bar steam at zero and 65 hours, and under 4 bar steam after 67 hours of operation.

The positive effect of higher steam (and total) pressure is observed in the I-V curves recorded for a composite anode cell under 1.5 and 4 bar steam on the anode side (**Figure *4***b) and keeping constant pO_2 and pH_2 on anode and cathode side, respectively. The operating voltage is decreased by 30-50 mV when the steam pressure is increased from 1.5 bar to 4 bar, reflecting an increased proton conductivity in the electrolyte, as inferred from the Nyquist plots presented in **Figure *4***c. The stability of the electrochemical performance after 65 hours of high-steam pressure operation is evidenced in the same figure.

The long-term stability of a tubular cell with BGLC/BZCY composite anode was further evaluated under pressurized electrolysis conditions (**Figure 5**a), showing excellent stability over 700 hours of operation at a constant current density of 62.5 $mAcm^{-2}$ with 1.5 bar steam on the anode. The small variations and spikes in the cell potential are associated with temperature and pressure changes that occurred upon refilling the steam supply water tank.

During operation, the pH_2O gradient over the cell will lead to a certain steam permeation due to ambipolar transport of protons and oxide ions, counteracted by the co-ionic migration of oxide ions towards the O_2/H_2O-side of the cell in electrolysis mode. The balance between ambipolar diffusion and co-ionic transport by oxide ions will establish a small water vapour partial pressure in the H_2 compartment, depending on the oxide ion transport number (i.e., T and pH_2O), ensuring hydration of the electrolyte there. The humidity in the H_2 exhaust gas stream from a cell operated at 600°C with 1.5 bar steam on the anode side was measured as a function of current density to evaluate water content in the produced hydrogen for the present cell and reactor design, shown in **Figure 5**b. As can be seen, the humidity of the

The energy efficiency of hydrogen production using tubular PCEs is presented as a function of current density in **Figure 5**c with four different assumptions; i) strict cell-level electrical efficiency assuming surplus free heat available, ii) energy efficiency including heat demand in endothermic operation, iii and iv) energy efficiency including water vaporization at 50% and 90% steam utilization, respectively. The present tubular PCEs with an active area of 12 cm^2 provide cell-level energy efficiencies above 80% at 150 $mAcm^{-2}$, with even higher efficiencies at lower current densities. From a technological perspective, it is needed to reduce the ohmic losses throughout the cell to yield similar efficiencies at current densities above 1 Acm^{-2}. This can be achieved through improved current collection along the length of the tube as well as implementing an electrolyte composition with higher dopant concentration and proton conductivity, e.g. BZCYYb or similar compositions.

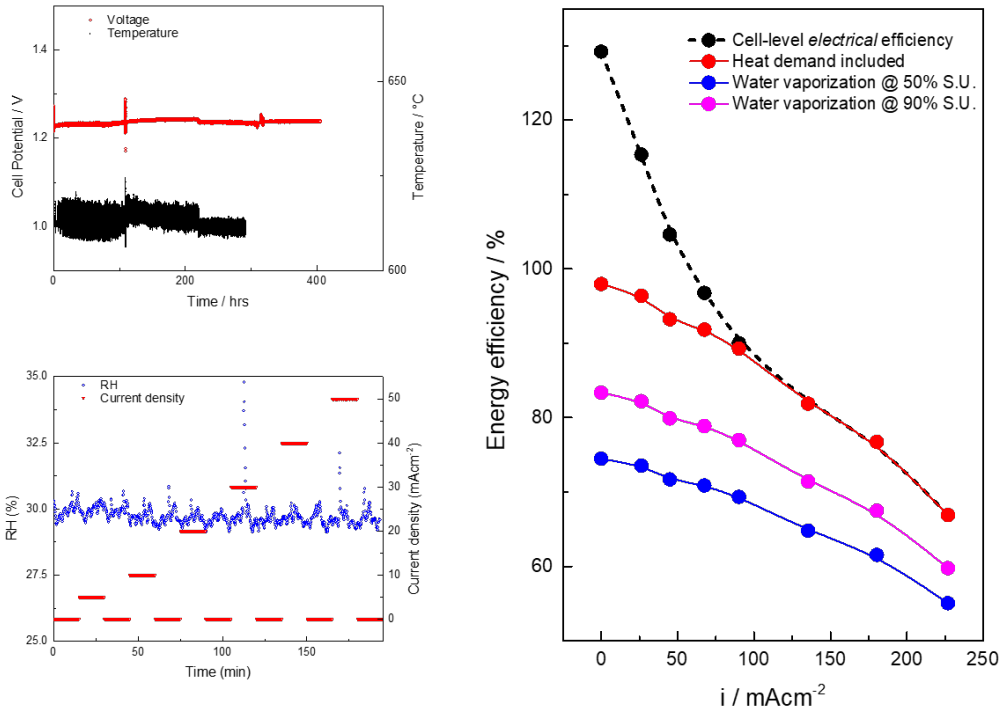

Figure 5:

To validate the observed positive effects of lowered R_p and higher pressure on the faradaic efficiency η_F of PCEs, a model is developed based on defect chemistry (Eq.1) and the Butler-Volmer relation for the electrode polarization. This model describes partial ionic and electronic currents as a function of cell potential (cf SI for details) with parameters from the literature for BZCY to describe transport through the electrolyte. The anode polarization resistance and total pressure (at a fixed steam utilization rate) are varied to investigate the effect of electrode performance and operating conditions. **Figure *6***a shows how the predicted faradaic efficiency increases significantly with decreasing R_p for a given current density, as the lower overpotential reduces the electron hole concentration in the electrolyte. The model also predicts increased faradaic efficiency at higher total pressures (**Figure *6***b) for a given steam utilization (SU) and charge transfer resistance. Thus, pressurized PCE operation allows improved performance and electrical efficiency and – contrary to conventional electrolysers – enable the production of dry electrochemically pressurized hydrogen directly in the cathode compartment without dilution with unreacted steam (SOE) or water drag (PEM) (**Figure *1***a).

Computational fluid-dynamics (CFD) modelling further reveals that the tubular design employed in this work allows for essentially isothermal operation along the entire tube length (**Figure *6***c-e). Furthermore, there are practically no radial concentration gradients, i.e. the proper gas-phase transport for the chosen cell geometry is confirmed, while the spatially-progressive steam conversion and dilution with the formed oxygen can be recognized (**Figure *6***f). Sensitivity analysis of the current density illustrates the transition between endo- and exothermic regimes along the cell length (SI Fig. 16a). The extended analysis on 29 cm-long cells – single or in-series segmented – shows again an isothermal profile along the tube length and absence of compositional gradients (SI Fig. 17a). These CFD results demonstrate that the electrolysis process is scalable for tubular PCE cells with beneficial heat and process integration.

To conclude, BGLC-based PCEs can be operated at a lower temperature and high faradaic efficiency, while the tubular geometry enables simple heat and process integration as well as low-cost cell fabrication and peripherals. As a consequence, the results presented herein demonstrate the potential of PCE technology as a cost-competitive alternative for large-scale energy storage and pressurized hydrogen production, especially when renewable or industrial waste heat is available.

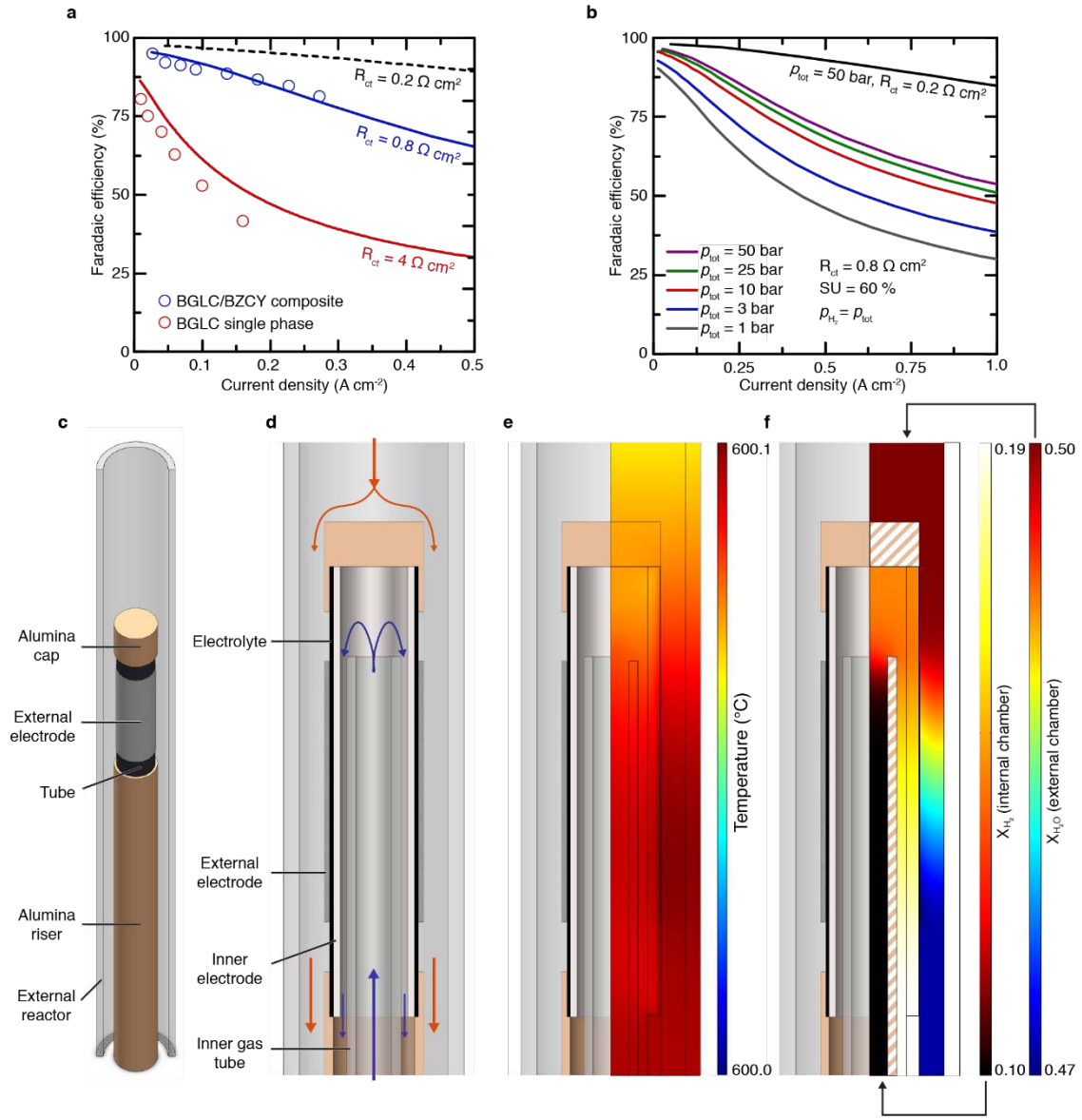

Figure 6: Charge transfer and CFD models of PCE system. Predicted faradaic efficiencies using Eq.1 (lines) as a function of charge transfer resistance (**a**) and total system pressure (**b**). The symbols in (**a**) represent the measured values for the single-phase and composite PCEs in this work. Results of the adiabatic CFD model are depicted in figures c-g. **c,** Description of the setup; **d,** Cross-section of the setup centered in the tube with a description of the external gas flow (orange arrows), and internal gas flow (blue arrows); **e,** Temperature profile for the reference case near the thermoneutral point; **f,** Molar fraction profiles for hydrogen in the internal chamber and for steam in the external chamber.

1 Hauch, A., Ebbesen, S. D., Jensen, S. H. & Mogensen, M. Highly efficient high temperature electrolysis. *Journal of Materials Chemistry* **18**, 2331-2340 (2008).

2 Laguna-Bercero, M. Recent advances in high temperature electrolysis using solid oxide fuel cells: A review. *Journal of Power Sources* **203**, 4-16 (2012).

3 Ebbesen, S. D., Jensen, S. H., Hauch, A. & Mogensen, M. B. High temperature electrolysis in alkaline cells, solid proton conducting cells, and solid oxide cells. *Chemical reviews* **114**, 10697-10734 (2014).
4 Knibbe, R., Traulsen, M. L., Hauch, A., Ebbesen, S. D. & Mogensen, M. Solid Oxide Electrolysis Cells: Degradation at High Current Densities. *Journal of The Electrochemical Society* **157**, B1209-B1217, doi:10.1149/1.3447752 (2010).
5 Hauch, A., Jensen, S. H., Ramousse, S. & Mogensen, M. Performance and Durability of Solid Oxide Electrolysis Cells. *Journal of The Electrochemical Society* **153**, A1741-A1747, doi:10.1149/1.2216562 (2006).
6 Wachsman, E. D. & Lee, K. T. Lowering the Temperature of Solid Oxide Fuel Cells. *Science* **334**, 935-939, doi:10.1126/science.1204090 (2011).
7 Ishihara, T., Jirathiwathanakul, N. & Zhong, H. Intermediate temperature solid oxide electrolysis cell using $LaGaO_3$ based perovskite electrolyte. *Energy & Environmental Science* **3**, 665-672 (2010).
8 Iwahara, H., Uchida, H. & Maeda, N. High temperature fuel and steam electrolysis cells using proton conductive solid electrolytes. *Journal of Power Sources* **7**, 293-301 (1982).
9 Norby, T. in *Perovskite oxide for solid oxide fuel cells Fuel Cells and Hydrogen Energy* (ed T. Ishihara) 217-241 (Springer, 2009).
10 Tong, J., Clark, D., Bernau, L., Sanders, M. & O'Hayre, R. Solid-state reactive sintering mechanism for large-grained yttrium-doped barium zirconate proton conducting ceramics. *Journal of Materials Chemistry* **20**, 6333-6341 (2010).
11 Iwahara, H., Yajima, T., Hibino, T., Ozaki, K. & Suzuki, H. Protonic conduction in calcium, strontium and barium zirconates. *Solid State Ionics* **61**, 65-69 (1993).
12 Duan, C. *et al.* Readily processed protonic ceramic fuel cells with high performance at low temperatures. *Science* **349**, 1321-1326 (2015).
13 Choi, S. *et al.* Exceptional power density and stability at intermediate temperatures in protonic ceramic fuel cells. *Nature Energy*, doi:10.1038/s41560-017-0085-9 (2018).
14 An, H. *et al.* A 5 × 5 cm2 protonic ceramic fuel cell with a power density of 1.3 W cm–2 at 600 °C. *Nature Energy*, doi:10.1038/s41560-018-0230-0 (2018).
15 Morejudo, S. *et al.* Direct conversion of methane to aromatics in a catalytic co-ionic membrane reactor. *Science* **353**, 563-566 (2016).
16 Malerød-Fjeld, H. *et al.* Thermo-electrochemical production of compressed hydrogen from methane with near-zero energy loss. *Nature Energy*, doi:10.1038/s41560-017-0029-4 (2017).
17 Babiniec, S. M., Ricote, S. & Sullivan, N. P. Characterization of ionic transport through $BaCe_{0.2}Zr_{0.7}Y_{0.1}O_{3-\delta}$ membranes in galvanic and electrolytic operation. *International Journal of Hydrogen Energy* **40**, 9278-9286, doi:https://doi.org/10.1016/j.ijhydene.2015.05.162 (2015).
18 Bi, L., Shafi, S. P. & Traversa, E. Y-doped $BaZrO_3$ as a chemically stable electrolyte for proton-conducting solid oxide electrolysis cells (SOECs). *Journal of Materials Chemistry A* **3**, 5815-5819, doi:10.1039/C4TA07202B (2015).
19 Li, S. & Xie, K. Composite Oxygen Electrode Based on LSCF and BSCF for Steam Electrolysis in a Proton-Conducting Solid Oxide Electrolyzer. *Journal of The Electrochemical Society* **160**, F224-F233, doi:10.1149/2.027303jes (2013).
20 Matsumoto, H., Sakai, T. & Okuyama, Y. in *Pure and Applied Chemistry* Vol. 85 427 (2012).
21 Gan, Y. *et al.* Composite Oxygen Electrode Based on LSCM for Steam Electrolysis in a Proton Conducting Solid Oxide Electrolyzer. *Journal of The Electrochemical Society* **159**, F763-F767, doi:10.1149/2.018212jes (2012).

22 Shang, M., Tong, J. & O'Hayre, R. A promising cathode for intermediate temperature protonic ceramic fuel cells: $BaCo_{0.4}Fe_{0.4}Zr_{0.2}O_{3-\delta}$. *RSC Advances* **3**, 15769-15775, doi:10.1039/C3RA41828F (2013).

23 Strandbakke, R. *et al.* Gd- and Pr-based double perovskite cobaltites as oxygen electrodes for proton ceramic fuel cells and electrolyser cells. *Solid State Ionics* **278**, 120-132, doi:http://dx.doi.org/10.1016/j.ssi.2015.05.014 (2015).

24 Poetzsch, D., Merkle, R. & Maier, J. Proton conductivity in mixed-conducting BSFZ perovskite from thermogravimetric relaxation. *Physical Chemistry Chemical Physics* **16**, 16446-16453 (2014).

25 Zohourian, R., Merkle, R. & Maier, J. Proton uptake into the protonic cathode material $BaCo_{0.4}Fe_{0.4}Zr_{0.2}O_{3-\delta}$ and comparison to protonic electrolyte materials. *Solid State Ionics* **299**, 64-69 (2017).

26 Strandbakke, R., Vøllestad, E., Robinson, S. A., Fontaine, M.-L. & Norby, T. $Ba_{0.5}Gd_{0.8}La_{0.7}Co_2O_{6-\delta}$ Infiltrated in Porous $BaZr_{0.7}Ce_{0.2}Y_{0.1}O_3$ Backbones as Electrode Material for Proton Ceramic Electrolytes. *Journal of The Electrochemical Society* **164**, F196-F202, doi:10.1149/2.0141704jes (2017).

27 Vollestad, E., Schrade, M., Segalini, J., Strandbakke, R. & Norby, T. Relating defect chemistry and electronic transport in the double perovsksite $Ba_{1-x}Gd_{0.8}La_{0.2+x}Co_2O_{6-\delta}$(BGLC). *Journal of Materials Chemistry A* **5**, 15743-15751, doi:10.1039/C7TA02659E (2017).

28 Brieuc, F., Dezanneau, G., Hayoun, M. & Dammak, H. Proton diffusion mechanisms in the double perovskite cathode material $GdBaCo_2O_{5.5}$: A molecular dynamics study. *Solid State Ionics* **309**, 187-191, doi:10.1016/j.ssi.2017.07.017 (2017).

29 Mokkelbost, T. *et al.* High-Temperature Proton-Conducting Lanthanum Ortho-Niobate-Based Materials. Part II: Sintering Properties and Solubility of Alkaline Earth Oxides. *Journal of the American Ceramic Society* **91**, 879-886, doi:10.1111/j.1551-2916.2007.02232.x (2008).

30 Tong, J., Clark, D., Hoban, M. & O'Hayre, R. Cost-effective solid-state reactive sintering method for high conductivity proton conducting yttrium-doped barium zirconium ceramics. *Solid State Ionics* **181**, 496-503, doi:https://doi.org/10.1016/j.ssi.2010.02.008 (2010).

31 Kwon, O. H. & Choi, G. M. Electrical conductivity of thick film YSZ. *Solid State Ionics* **177**, 3057-3062, doi:https://doi.org/10.1016/j.ssi.2006.07.039 (2006).

32 Timakul, P., Jinawath, S. & Aungkavattana, P. Fabrication of electrolyte materials for solid oxide fuel cells by tape-casting. *Ceramics International* **34**, 867-871, doi:https://doi.org/10.1016/j.ceramint.2007.09.038 (2008).

33 Kim, S. J., Kim, K. J., Dayaghi, A. M. & Choi, G. M. Polarization and stability of $La_2NiO_{4+\delta}$ in comparison with $La_{0.6}Sr_{0.4}Co_{0.2}Fe_{0.8}O_{3-\delta}$ as air electrode of solid oxide electrolysis cell. *International Journal of Hydrogen Energy* **41**, 14498-14506, doi:https://doi.org/10.1016/j.ijhydene.2016.05.284 (2016).

34 Jacobsen, T., Chatzichristodoulou, C. & Mogensen, M. B. Fermi potential across working solid oxide cells with zirconia or ceria electrolytes. *ECS Transactions* **61**, 203-214 (2014).

35 Zhu, H. & Kee, R. J. Membrane polarization in mixed-conducting ceramic fuel cells and electrolyzers. *International Journal of Hydrogen Energy* **41**, 2931-2943, doi:https://doi.org/10.1016/j.ijhydene.2015.10.100 (2016).